4720–4727 Nucleic Acids Research, 2002, Vol. 30 No. 21

Scanning confocal fluorescence microscopy for single molecule analysis of nucleotide excision repair complexes

G. M. J. Segers-Nolten*, C. Wyman[1,2], N. Wijgers[1], W. Vermeulen[1], A. T. M. Lenferink, J. H. J. Hoeijmakers[1], J. Greve and C. Otto

Department of Applied Physics, Biophysical Technology Group, Biomedical Technology Institute, University of Twente, PO Box 217, 7500 AE Enschede, The Netherlands, [1]Department of Cell Biology and Genetics, Erasmus MC, PO Box 1738, 3000 DR Rotterdam, The Netherlands and [2]Department of Radiation Oncology, University Hospital Rotterdam-Daniel, Rotterdam, The Netherlands

Received June 26, 2002; Revised and Accepted September 12, 2002

ABSTRACT

We used scanning confocal fluorescence microscopy to observe and analyze individual DNA–protein complexes formed between human nucleotide excision repair (NER) proteins and model DNA substrates. For this purpose human XPA protein was fused to EGFP, purified and shown to be functional. Binding of EGFP-labeled XPA protein to a Cy3.5-labeled DNA substrate, in the presence and absence of RPA, was assessed quantitatively by simultaneous excitation and emission detection of both fluorophores. Co-localization of Cy3.5 and EGFP signals within one diffraction limited spot indicated complexes of XPA with DNA. Measurements were performed on samples in a 1% agarose matrix in conditions that are compatible with protein activity and where reactions can be studied under equilibrium conditions. In these samples DNA alone was freely diffusing and protein-bound DNA was immobile, whereby they could be discriminated resulting in quantitative data on DNA binding. On the single molecule level ~10% of XPA co-localized with DNA; this increased to 32% in the presence of RPA. These results, especially the enhanced binding of XPA in the presence of RPA, are similar to those obtained in bulk experiments, validating the utility of scanning confocal fluorescence microscopy for investigating functional interactions at the single molecule level.

INTRODUCTION

Techniques for observing and manipulating single molecules (1–6) offer new perspectives to study biological mechanisms. Observation and analysis of protein–DNA interactions at the single molecule level can provide information on macromolecular interactions that cannot be obtained from standard bulk *in vitro* assays. For instance, the behavior of individual molecules can be followed, the stochastic properties of interactions recorded and subpopulations of complexes can be identified whereby their distribution provides information on mechanistic possibilities. For complex reactions involving many components, active species may be rare but can still be identified and analyzed by single molecule methods. We have developed a scanning confocal fluorescence microscopy (7) method that can detect single fluorophores and allows the study of single molecule interactions between proteins and DNA under physiological conditions.

Scanning confocal fluorescence microscopy is particularly attractive since high detection sensitivity and sufficient reduction of background signal allow the observation of individual fluorescent molecules. Our home-built scanning confocal fluorescence microscope offers the possibility to simultaneously excite different fluorophores at their specific excitation wavelengths. In addition, with a single scan multiple fluorescence emission wavelengths from specific molecules can be detected at the same time. With this procedure the molecules of interest are not influenced by physical interaction with a scanning probe. In contrast, other single molecule techniques, like AFM (8–10) or NSOM (11,12), require a probe in very close proximity to the sample, which may result in undesirable interactions. Another advantage of single molecule studies using scanning confocal microscopy is that samples can be prepared in such a way that equilibrium reaction conditions are maintained during scanning. The application of gel matrices to immobilize molecules during imaging has proven to be a useful tool (13–16). The properties of the gel are selected in such a way that our relevant, small DNA molecules freely diffuse through the gel; protein molecules, however, are immobile (13–16). DNA becomes immobilized upon interaction with protein. The confinement of protein molecules in the pores of a gel has several advantages over immobilization on a surface. Using water-based agarose gels (13,14) the functionality of

*To whom correspondence should be addressed. Tel: +31 53 489 3358; Fax: +31 53 489 1105; Email: g.m.j.segers-nolten@tn.utwente.nl

molecules is preserved, influence from interactions with a surface is avoided and it provides a convenient way to control sample concentration. Together the features mentioned make scanning confocal fluorescence microscopy especially useful to study intricate DNA–protein interactions at the single molecule level.

Here we have investigated protein–DNA complexes involved in nucleotide excision repair (NER). NER is one of the most important mammalian DNA repair processes responsible for removing a wide variety of helix-distorting lesions from genomic DNA (17–20). Genetic studies have identified the gene products required for NER in humans. Biochemical analysis has produced a general outline of the mechanism, which includes recognition of DNA lesions, unwinding of the DNA double helix around the damage, interaction of several factors bound to DNA that verify the damage and, finally, excision of a 24–29 nt piece of DNA including the damaged bases (19). This process involves the ordered assembly of several proteins at a specific DNA site and undoubtedly requires complex intermediate structures. The exact composition and lifetime of the various intermediate structures, and thus the precise reaction mechanism, is not known. This is in part due to a lack of methods to identify distinct intermediate structures (DNA–protein complexes) in a mixture of different species, quantify their prevalence and determine their lifetime.

In order to develop methods to address some of the questions raised above we initiated single molecule studies of the interactions of NER proteins with a model DNA substrate (21). To see whether scanning confocal fluorescence microscopy of single molecules embedded in gel matrices provides valid information on the dynamics of protein–DNA complex assembly we used a relatively simple DNA–(NER)protein complex which has already been characterized in bulk biochemical experiments. We first analyzed the interaction of human XPA protein with a 90 bp double-stranded DNA molecule that has a central 30 nt unpaired region, subsequently referred to as 'bubble DNA'. XPA plays a crucial role in NER and binds to bubble DNA (22,23). In addition, RPA is known to enhance the binding of XPA to DNA (22–29). This protein–DNA complex is suggested to be important for damage verification and proper orientation of excision activities (30). To visualize individual components with scanning confocal fluorescence microscopy, both DNA and XPA were fluorescently labeled. One DNA strand was 5′-labeled with a single Cy3.5 molecule. EGFP was fused in-frame to XPA, which was then overproduced in *Escherichia coli* and purified to near homogeneity. The measured affinity of XPA for this DNA substrate and the influence of RPA on this affinity, as determined here using single molecule scanning confocal fluorescence microscopy, are in good agreement with results obtained from bulk biochemical methods. Moreover, we show that the applied procedure of DNA immobilization by protein binding in a gel is very well suited for single molecule protein–DNA binding studies in general. Our results demonstrate that single molecule spectroscopic imaging is a promising new technique that will allow us to identify and study the dynamic interactions of intermediates in NER. This method also has the potential to provide new insights into the mechanism of other complex DNA transactions.

MATERIALS AND METHODS

Production and purification of His_9HA–EGFP-tagged XPA

EGFP-tagged XPA was generated by fusing the cDNA coding for enhanced green fluorescent protein (EGFP) to *XPA* cDNA. The entire *XPA* gene, except the first three amino acids, was cloned in-frame into the EGFP-C1 vector (U55763; Clontech). In addition, an extra sequence encoding for both a nine histidine (His_9) stretch and a HA epitope were added to the N-terminal coding part of EGFP. With that aim, a double-stranded oligonucleotide was inserted 5′ of EGFP (coding strand, 5′-CT AGC AAC ATG GGC CAC CAC CAT CAC CAT CAT CAC CAC CAC GGC **TAC CCA TAC GAT GTT CCA GAT TAC GCA AGC** GC-3′). The resulting fusion gene, consisting of a nine histidine stretch (underlined), HA tag (bold) and EGFP–XPA, was excised from the C1 vector and ligated in the pET28 vector (Novagen) for bacterial expression, resulting in the His_9HA–EGFP–XPA–pet28 (hereafter EGFP–XPA) construct.

This recombinant plasmid was transformed into the *E.coli* host BL21(DE3)LysS. Prior to protein overexpression, cells were grown in 1 l of phosphate-buffered LB (1.5 g/l NaCl, 10 g/l tryptone, 5 g/l yeast extract, 7 g/l $Na_2HPO_4{\cdot}2H_2O$ and 0.5 g/l KH_2PO_4) to an OD_{600} of 0.6, collected by centrifugation and resuspended in fresh medium including 0.4% glucose. Protein expression was induced with 2 mM IPTG for 3 h at 28°C. Cells were collected by centrifugation, washed with phosphate-buffered saline (PBS) and frozen in 20 ml of PBS, 10% glycerol. To isolate the recombinant protein, cells were thawed and resuspended in 7.5 ml of PBS, containing 0.01% NP-40, 2 mM Pefabloc, and subsequently lysed by sonication. The whole cell extract was cleared from insoluble particles by centrifugation for 45 min at 19 000 r.p.m. at 4°C. Next, 40 ml of the supernatant was loaded on a 20 ml heparin–Sepharose column, prewashed and equilibrated with buffer A (PBS, 0.01% NP-40, 1 mM β-mercaptoethanol, 10% glycerol). Unbound proteins were washed off using buffer A. The bound proteins were eluted with a 10 column vol linear gradient of buffer A to buffer B (buffer A + 1 M NaCl). Fractions of 4 ml were collected and tested for the presence of EGFP–XPA by western blot analysis. EGFP–XPA eluted at ~400 mM NaCl. Fractions containing the EGFP–XPA fusion protein were pooled and loaded on a 3 ml phosphocellulose column (Whatmann). Unbound proteins were removed by washing with 10 column vol of PBS supplemented with 0.65 M NaCl; subsequently proteins were eluted with 1.2 M NaCl. Peak fractions were pooled, 5 mM imidazole and Pefabloc (Merck) were added and the fractions subsequently bound to 1 ml of Ni–NTA agarose beads (Qiagen) (pre-washed with PBS, 5 mM imidazole). The column was washed with 5 column vol of buffer C (25 mM HEPES, 0.01% NP-40, 10% glycerol, Pefabloc, 1 mM β-mercaptoethanol, 0.1 M KCl) containing, respectively, 5, 20 and 60 mM imidazole and eluted with buffer C containing 200 mM imidazole. Protein fractions at each stage during production and purification were analyzed by standard SDS–PAGE (11%), Coommassie brilliant blue staining and immunoblotting using rabbit anti-XPA IgG (Santa Cruz) or mouse monoclonal anti-HA (12CA5) and secondary goat anti-rabbit antibody (BIOSOURCE)

conjugated to alkaline phosphatase. The recombinant human RPA complex utilized in our studies, purified from *E.coli* cells, was kindly provided by M. Modesti and A. Janicijevic (Genetics, Rotterdam, The Netherlands) (31,32).

Microinjection and DNA repair synthesis

The activity of the purified EGFP–XPA protein was assayed by microinjecting fractions into XPA-deficient human fibroblasts (XP25RO) and subsequently testing the DNA repair capacity, as described previously (33). After injection the cells were incubated for 15 min at 37°C in standard medium to recover from the injections. Fluorescent (EGFP) images were obtained with an Olympus IX70 microscope, PlanApo 60×/1.40 oil immersion lens (excitation at 455–490 nm and emission detection with a 510 nm long pass filter).

After microinjection and fluorescent image recording, DNA repair capacity was determined by measuring unscheduled DNA synthesis (UDS) (33). Human fibroblasts were UV-irradiated (16 J/m^2, 254 nm), labeled for 2 h using [^{3}H]thymidine (20 μCi/ml) and fixed for autoradiography. Autoradiographic grains above the nuclei of injected polykaryons were counted and compared with the number of grains above nuclei of wild-type fibroblasts (C5RO) assayed in parallel.

DNA substrate

DNA substrates that model NER intermediates were prepared from a pair of 90 nt oligomers, one of which had a 5′ Cy3.5 label (Biozym, Landgraaf, The Netherlands). The sequence of the oligomers was the same as described in Matsunaga *et al.* (21). Upon annealing equimolar amounts of 90mers in 25 mM HEPES pH 7.5, 100 mM NaCl, 10 mM $MgCl_2$, at a final concentration of 10^{-6} M, double-stranded DNA with a central 30 bp unpaired region, bubble DNA substrate, was produced. Formation of bubble DNA was checked by electrophoresis in an 8% non-denaturing polyacrylamide gel and ~91% was determined to be in the bubble configuration. The bubble DNA was used without further purification.

Binding reactions

EGFP–XPA/DNA complexes were prepared by combining DNA bubble substrate and EGFP–XPA at a molar ratio of 20:1. During incubation the EGFP–XPA concentration was ~3×10^{-9} M and DNA concentration was 6×10^{-8} M in a 5.3 μl volume of 25 mM HEPES, 40 mM KCl, 60 mM NaCl, 7 mM $MgCl_2$, 0.4 mM DTT, 0.02% NP-40, 2.6% glycerol, pH 7.5. For preparation of XPA/RPA/DNA complexes DNA, EGFP–XPA and RPA were combined as above in a molar ratio of 20:1:1. Binding reactions were incubated for 30 min at room temperature.

Sample preparation for confocal fluorescence microscopy

For single molecule confocal measurements, proteins and reactions containing complexes of protein and DNA were diluted to concentrations of ~5×10^{-10} M with respect to EGFP–XPA at 30°C in molten low melt agarose, 1% (w/v) in 25 mM HEPES, 40 mM KCl, 60 mM NaCl, 7 mM $MgCl_2$, pH 7.5. The agarose mixture was sandwiched between two quartz coverslips, diameter 25 mm. Adsorption of bubble DNA only was achieved by applying 10 μl of a 10^{-9} M solution of Cy3.5-labeled DNA in buffer between two 25 mm diameter quartz coverslips.

Scanning confocal microscopy

We have constructed a scanning confocal microscope for single molecule studies in which excitation light is provided by a mixed gas Ar–Kr laser (Innova 70; Coherent). The excitation light is focused onto the sample by a water immersion objective (C-Apochromat 63×, 1.20 NA; Zeiss). The reflected light is collected by the same objective and directed onto two avalanche photodiodes (APDs) by a dichroic beamsplitter. The spectrally separated emissions are focused onto 25 μm pinholes, which are present in front of both APDs. Emission filters are used for selection of the proper emission wavelengths. Reflected excitation wavelengths are suppressed by notch filters. The sample is scanned in two directions by a computer controlled piezoelectric scanning system, composed of an electronic position controller (E-500; Physik Instrumente, Waldbronn, Germany) and a scanning stage (P-740.20, 50 × 50 μm; Physik Instrumente).

LabVIEW software (National Instruments, Austin, TX) is used to program and perform image acquisition. For spectral separation of Cy3.5 and EGFP fluorescence a 565DCXR dichroic beamsplitter is used. The emission filter for EGFP is an HQ525/50m filter and for Cy3.5 it is a D605/55m filter. All filters and dichroic beamsplitters were purchased from Chroma Technology Corp. (Brattleboro, VT).

In addition to imaging by scanning, the set-up also offers the possibility to exactly position the scanner so that a single molecule is in focus for a defined time. In this way, a time trace of the fluorescence behavior of a single molecule can be recorded with a time resolution of 10 μs.

RESULTS

In order to obtain a fluorescent NER protein we fused EGFP to XPA at the DNA level. Both a nine times histidine repeat and HA epitope tag were added to the N-terminus of EGFP to aid in protein purification and immunological detection. The cDNA coding for recombinant His_9HA–EGFP–XPA under control of the CMV enhancer/promoter was microinjected into XPA-deficient cells to test for biological activity. This hybrid cDNA was able to fully complement the severe NER defect of XP group A cells (data not shown), indicating that the EGFP tag does not interfere with XPA function. For bacterial expression, the hybrid cDNA was excised and inserted in an IPTG-inducible expression cassette (pET28).

EGFP–XPA was purified from *E.coli* strain BL21(DE3)-LysS, harboring the pET28-EGFP-XPA plasmid. As shown in Figure 1, a protein migrating at the expected position for the tagged XPA in SDS–PAGE was visible (arrow, lanes D and E). Because of the known aberrant mobility of XPA in SDS–PAGE the His_9HA–EGFP–XPA fusion protein appears as a protein with higher molecular weight than the calculated 62.5 kDa. Immunoblot analyis, using XPA-specific antibodies, confirmed that indeed the desired fusion product was induced (data not shown). For each of the subsequent steps of purification, respectively, heparin–Sepharose, phosphocellulose and Ni–NTA agarose, purity and yield of the fusion protein were monitored by gel staining (Fig. 1) and immunoblotting. The elution fractions of the last purification

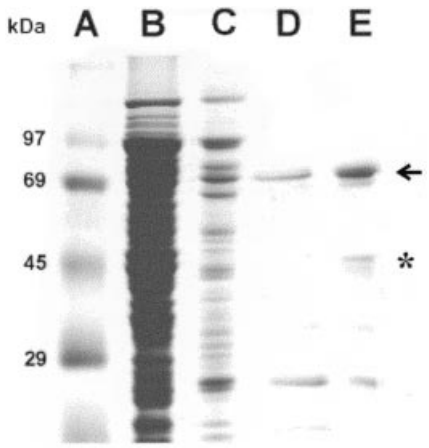

Figure 1. Protein profile of EGFP–XPA purification. Purification of EGFP–XPA was followed by loading samples of fractions from the purification steps on SDS–PAGE gels and staining with Coomassie brilliant blue. Lane A, standard prestained molecular weight markers (Gibco BRL, catalog no. 26041-020); molecular size is indicated in kDa. Lane B, crude extract. Lane C, fractions eluted from the heparin column and loaded onto the phosphocellulose column. Lane D, fractions eluted from the phosphocellulose column and loaded onto the Ni–NTA column. Lane E, fraction eluted from the Ni–NTA column with 200 mM imidazole. The arrow indicates the fusion protein His, HA–EGFP–XPA, running at ~70 kDa. A minority of the fusion protein is degraded, as shown by the asterisk, likely free XPA (without the GFP tag), since it cross-reacts with anti-XPA in western blotting (not shown).

step contained predominantly intact EGFP–XPA polypeptide with some proteolytic degradation products.

The isolated recombinant polypeptide (>95% purity) was tested for its biological activity. With that aim the protein was introduced, via microneedle injection, into XPA-deficient cells. NER activity of the injected cells was measured by determining DNA repair synthesis after UV-irradiation (UDS). Within 15 min after microinjection, a bright fluorescent signal was observed in the nuclei of the majority of injected cells. After fluorescence image recording, cells were assayed for their repair activity. The cells with green fluorescent nuclei were also corrected (up to wild-type levels) for the severe UDS defect present in XP-A cells. The number of autoradiographic grains above the injected cell nuclei was significantly higher than above the non-injected neighboring cells (data not shown) and comparable to results from microinjection with non-tagged XPA (34). Both nuclear targeting and the complete restoration of UDS indicate that the His_9HA–EGFP tag does not interfere with the proper function of XPA and that the purified protein is biologically active. In conclusion, both the purity and the biological activity indicate that this protein is a bona fide NER reagent to be applied in single molecule studies.

Imaging single EGFP–XPA proteins

To image single fluorescent molecules by scanning confocal fluorescence microscopy it is necessary to immobilize these molecules during the scanning interval. For this purpose we used an agarose gel matrix, which offers the advantage of working in buffer and the ability to control the concentration of molecules in the sample. Figure 2B is a scanning confocal image of EGFP–XPA molecules immobilized in a 1% agarose gel; emission was detected between 500 and 550 nm. The

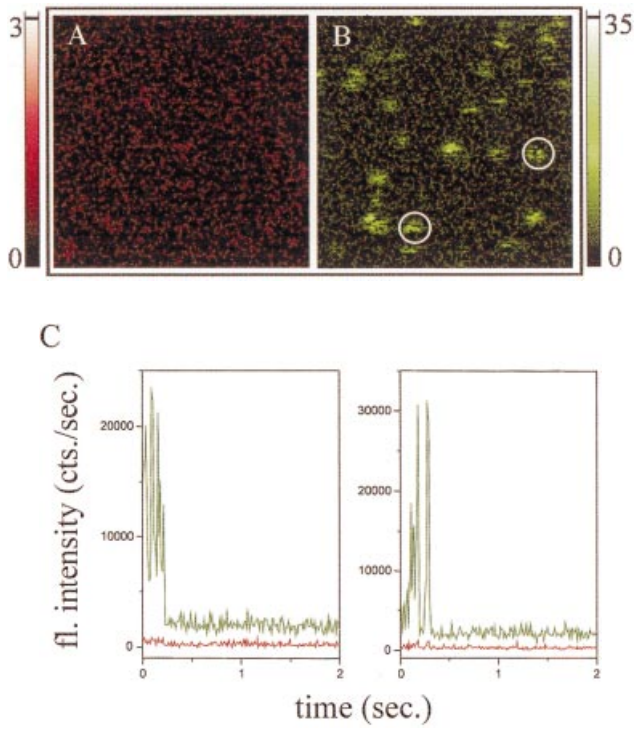

Figure 2. Confocal results of individual EGFP–XPA molecules immobilized in a 1% agarose gel. (**A**) Confocal image recorded from EGFP emission detected in the Cy3.5 detection channel, 577–632 nm region. (**B**) Confocal image recorded from EGFP emission detected in the EGFP detection channel, 500–550 nm region. Image size is 6.2 × 6.2 µm, 128 × 128 pixels, integration time is 0.5 ms/pixel. (**C**) Representative time traces of individual EGFP–XPA molecules measured simultaneously in both detection channels, integration time 10 ms. The left time traces were measured at the lower left circled position, the right time traces at the upper right circled position in (B). The fluorescence behavior in the Cy3.5 detection channel is indicated in red, the fluorescence behavior in the EGFP detection channel is in green. Excitation was 4 kW/cm^2 at 488 nm.

bright spots in this image represent the emission profiles from immobilized EGFP–XPA molecules that can easily be distinguished from background signal. The observed one-step bleaching and blinking (characteristic for GFP) behavior (35–37), as detected by acquiring time traces (Fig. 2C), strongly suggests that fluorescent spots are derived from single molecule emission. This behavior, together with the expected fluorescence intensity level, confirms that we were observing individual EGFP–XPA molecules. Simultaneously with the image in Figure 2B, an image was recorded from the EGFP sample with the detection wavelength in the 577–632 nm region, the detection window for Cy3.5 emission (Fig. 2A). The low intensity of this image and the absence of localized spots show that there is virtually no cross-talk from EGFP emission into the Cy3.5 detection channel.

Imaging bubble DNA

In contrast to EGFP–XPA molecules, 90 bp bubble DNA molecules are not immobilized in a 1% agarose matrix. The images obtained after scanning of Cy3.5-labeled bubble DNA molecules alone in a 1% agarose matrix (Fig. 3A) showed only diffusing DNA molecules. For comparison, Figure 3B is a confocal image of Cy3.5-labeled bubble DNA molecules

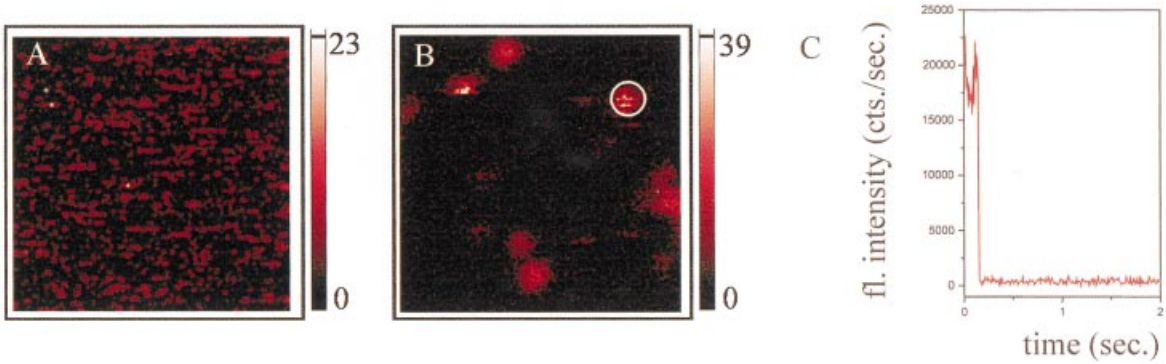

Figure 3. Confocal results of Cy3.5–bubble DNA molecules. Images are recorded from Cy3.5 emission detected in the Cy3.5 detection channel, 577–632 nm region. (**A**) In 1% agarose. (**B**) Adsorbed to quartz. Image size is 6.2 × 6.2 μm, 128 × 128 pixels, integration time 0.5 ms/pixel. (**C**) Typical time trace of an individual Cy3.5–bubble DNA molecule measured at the circled position in (B) with an integration time of 10 ms and emission detection from 577 to 632 nm. Excitation was 4 kW/cm^2 at 568 nm.

immobilized on quartz. Again, the time trace of a representative fluorescent spot (Fig. 3C) shows signal intensity and sudden bleaching characteristic of a single Cy3.5 molecule. Because we know from the image in Figure 2B that EGFP–XPA is immobilized in 1% agarose, we presume that after binding of EGFP–XPA protein to the DNA, the DNA will also be immobilized.

Single molecule imaging of EGFP–XPA/bubble DNA complexes

EGFP–XPA was incubated with Cy3.5–bubble DNA as described, after which the mixture was diluted to a concentration of ~5 × 10^{-10} M EGFP–XPA in 1% agarose and prepared for scanning confocal fluorescence microscopy. Images were recorded simultaneously for the Cy3.5 and the EGFP fluorescent labels (Fig. 4A and B, respectively). The apparent co-localization of Cy3.5 and EGFP signals within the same diffraction limited spot indicates that a DNA molecule is trapped by EGFP–XPA, suggesting the presence of a complex between XPA and the bubble DNA. DNA unbound by protein is still freely diffusing in the agarose matrix. A control experiment in which we combined pure EGFP with bubble DNA did not result in any immobilization of DNA (data not shown). Complex formation was assessed quantitatively by determining the percentage of EGFP–XPA spots that co-localized with Cy3.5. From analysis of 361 pairs of images containing in total 4340 EGFP–XPA molecules, we observed that a 10.1% fraction of EGFP–XPA molecules co-localized with Cy3.5–bubble DNA, indicating XPA–DNA complexes. This fraction of EGFP–XPA/bubble DNA complexes corresponds to an equilibrium dissociation constant K_d of 89 nM, taking into account the actual concentrations in the sample during measurement, 5 × 10^{-10} M for EGFP–XPA and 10^{-8} M for DNA. Recently, fluorescence anisotropy (22) has been used to determine the equilibrium dissociation constant for XPA binding to DNA. With that method, an equilibrium dissociation constant of 380 nM was determined. However, the applied experimental conditions were significantly different from ours. They used 36 bp DNA with a 6 nt bubble in reaction buffer without KCl containing 2 mM $MgCl_2$, where we used 40 mM KCl together with 7 mM $MgCl_2$. Nevertheless, the binding constant for XPA–DNA interaction

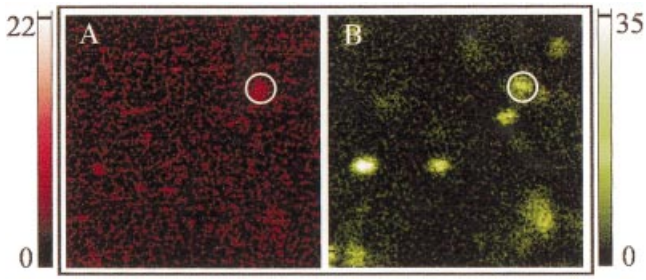

Figure 4. Confocal images from complexes of EGFP–XPA and Cy3.5–bubble DNA (ratio 1:20) in a 1% agarose matrix with simultaneous excitation and emission detection of the EGFP and Cy3.5 labels. (**A**) Cy3.5 emission, 577–632 nm; (**B**) EGFP emission, 500–550 nm. Image size is 6.2 × 6.2 μm, 128 × 128 pixels, integration time 0.5 ms/pixel, excitation 4 kW/cm^2 at both 488 and 568 nm. The circled position indicates the presence of a complex between EGFP–XPA and Cy3.5–bubble DNA.

that we determined here is well within the large range of K_d values obtained by more established bulk methods, varying from several nanomolar to even micromolar concentrations (22,27–29).

RPA stabilizes the EGFP–XPA/bubble DNA complexes

Although we were able to detect binding of XPA to a bubble DNA substrate, it does so with a relatively weak association constant. Several studies employing standard biochemical measurements have demonstrated that RPA enhances the binding of XPA to various DNA substrates (22–26,28,29,38). We tested the ability of our single molecule scanning confocal fluorescence microscope to detect this RPA-induced stabilization of XPA–DNA complexes. EGFP–XPA, RPA and DNA were combined in binding reactions as described in Materials and Methods before immobilization in agarose and confocal imaging. Images registering fluorescence simultaneously from EGFP–XPA and Cy3.5–DNA were collected and the percentage of XPA–DNA complexes determined from the co-localizing spots. As shown in two representative image pairs in Figure 5, the number of complexes, indicated by the number of co-localized spots, is higher with RPA than in the presence of XPA alone (compare with Fig. 4). In Figure 6 representative time traces of the fluorescence emission in two channels are

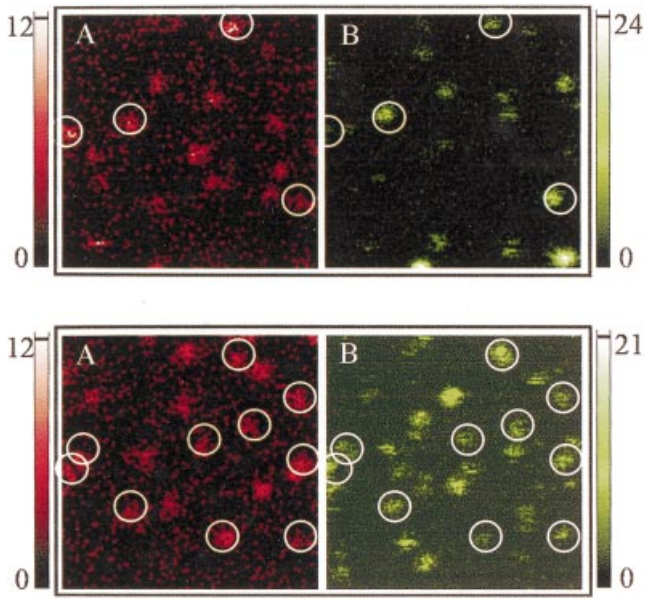

Figure 5. Scanning confocal images from complexes of EGFP–XPA, RPA and Cy3.5–bubble DNA (ratio 1:1:20) in a 1% agarose matrix with simultaneous excitation and emission detection of the EGFP and Cy3.5 labels. (**A**) Cy3.5 emission, 577–632 nm; (**B**) EGFP emission, 500–550 nm. Image size is 6.2 × 6.2 μm, 128 × 128 pixels, integration time 0.5 ms/pixel, excitation 4 kW/cm^2 at both 488 and 568 nm. Circled positions indicate co-localization of EGFP–XPA and Cy3.5–bubble DNA.

shown in which co-localization of the EGFP and Cy3.5 signals can be observed. From analysis of 351 pairs of images, including 4352 EGFP–XPA molecules, we observed 31.8% of the XPA to be bound to DNA in the presence of RPA. This confirms the previously reported enhancement by RPA of the binding of XPA to different DNA substrates (22–26,28,29,38). The corresponding K_d for binding of XPA in the presence of RPA to bubble DNA is calculated to be 21 nM. There is, however, no published data available from equilibrium binding experiments to directly compare this number with. In other studies different DNA substrates and salt conditions were used, as well as affinity tagged and untagged versions of proteins (39,40).

We also observe immobilized bubble DNA molecules in Figure 5A that do not co-localize with EGFP–XPA fluorescence. From the fact that these DNA molecules are not freely diffusing we conclude that they are likely in complex with RPA only. Analysis of the images reveals that on average 71.9% of the immobilized protein-bound DNA molecules are immobilized by EGFP–XPA or by the combination of EGFP–XPA and RPA. Consequently, 28.1% of the protein-bound DNA fraction includes no fluorescent protein and is likely RPA–DNA complexes. In the determination of this fraction we should, however, consider that our EGFP–XPA contains a small fraction of degradation products, free XPA and EGFP (Fig. 1). The unlabeled XPA present might still be able to bind to DNA and in this way contribute to the immobilized DNA fraction without showing an accompanying EGFP signal. Also, the fluorescence capacity of part of the EGFP-labeled XPA molecules may have been lost. However, in the absence of RPA, the EGFP–XPA binding experiments with bubble DNA resulted in only a low number of immobilized DNA molecules, non-co-localizing with EGFP (Fig. 4). This means that the fraction of XPA present either as unlabeled or non-fluorescent protein does not make a significant contribution in the binding experiments. Indeed, specific binding of RPA to DNA bubble substrates has been reported (21), with a 30 nt bubble being the minimum size for high affinity RPA binding (41). Our results show that DNA immobilization can be used for the quantitative determination of protein–DNA binding even when the protein is non-fluorescent, like the RPA protein used.

DISCUSSION

Here we show that we have established a single molecule monitoring procedure using scanning confocal fluorescence microscopy on agarose gel-based samples to visualize and quantify biomolecular interactions under physiological and equilibrium conditions. As a model system we used a well-defined reaction intermediate from the NER pathway, i.e. binding of the damage verifiers XPA and RPA to a double-stranded DNA duplex containing a 30 nt bubble. We used a 5′ Cy3.5 fluorescently labeled DNA substrate and GFP-tagged

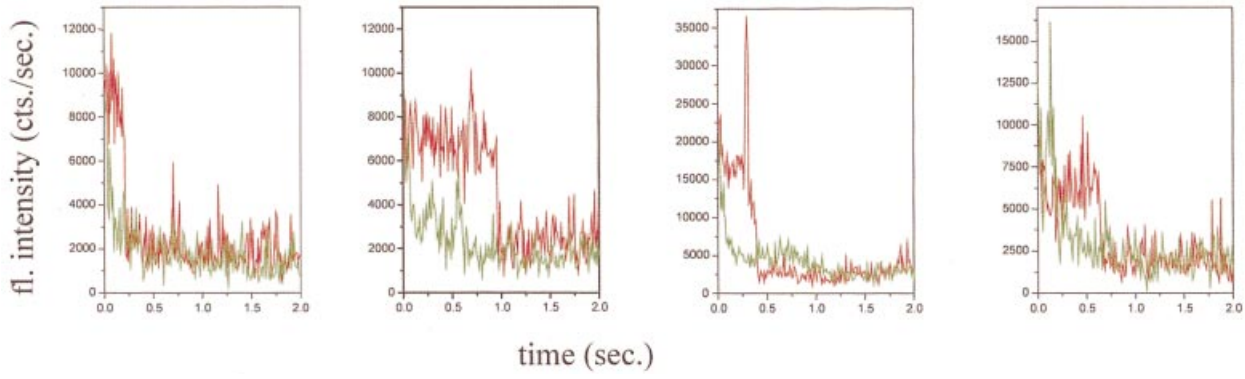

Figure 6. Representative time traces measured simultaneously in both detection channels at positions of co-localized EGFP and Cy3.5 signal with an integration time of 10 ms. The fluorescence behavior in the Cy3.5 detection channel is indicated in red, the fluorescence behavior in the EGFP detection channel is in green. Excitation was 4 kW/cm^2 at both 488 and 568 nm.

XPA, which was overproduced in *E.coli*, purified to near homogeneity and shown to be fully functional in *in vivo* NER.

The properties of the gel are such that protein-bound DNA can be easily distinguished from unbound DNA. Uncomplexed DNA bubble substrates diffuse freely within the agarose matrix. Binding to proteins results in DNA immobilization, which can be quantified. After assembly of protein–DNA complexes, co-localization of the GFP label (attached to the XPA protein) with the Cy3.5 label on the DNA is observed by simultaneously exciting both fluorophores and detecting the emission in two spectrally separated channels. Because the concentration of the components can be controlled and their interaction quantified, this method should be widely applicable to the study of protein–DNA interactions at the single molecule level in equilibrium conditions.

The observed low affinity of XPA for bubble DNA, as determined here on the single molecule level, is in agreement with already reported binding affinities from biochemical methods (22,27–29). Also, the enhancement of XPA binding by the RPA protein is in good correspondence with results reported from ensemble measurements (22–26,28,29,38). So far only one single molecule study has been published on NER proteins. In this study autocorrelation methods were applied to reveal conformational dynamics of individual XPA–DNA complexes on two different time scales (42). A 55 bp double-stranded DNA substrate was used with a 5′-fluorescein considered as a lesion for DNA repair. The difference in approach as well as the interest in other aspects of individual NER complexes makes it difficult to compare with our results. From biochemical methods it has been demonstrated that the bubble DNA substrate used is a relevant model substrate for some steps of the NER mechanism (21). The XPA–DNA binding reaction studied here is obviously only a starting point for single molecule analysis of the NER reaction. We expect to obtain new information on the NER mechanism studying authentic NER-specific damages and additional protein components.

We can conclude from our results so far that complicated biological processes, like NER, can be analyzed on a single molecule level using confocal fluorescence microscopy and GFP fusion proteins. In future experiments we plan to extend our studies to describe the dynamics of interactions between NER components and DNA. In addition, our home-built microscope set-up is able to measure the dynamics and properties of single macromolecular interactions, using fluorescence resonance energy transfer between proper spectral variants of GFP (such as CFP and YFP) fused to different NER proteins (14). The time resolution of data acquisition in our set-up allows us to determine interaction dynamics on a time scale of 10 μs. Our results so far and the planned expansion to dynamic studies clearly indicate an exciting future role for single molecule confocal fluorescence microscopy to provide new insights into the molecular mechanisms of vital biological reactions.

ACKNOWLEDGEMENTS

This work was financially supported by the Dutch Technology Foundation (STW), grant TTN.4821, SON-SLW (grant 805.49.002) and a SPINOZA award from NWO.

REFERENCES

1. Weiss,S. (1999) Fluorescence spectroscopy of single biomolecules. *Science*, **283**, 1676–1683.
2. Ishijima,A. and Yanagida,T. (2001) Single molecule nanobioscience. *Trends Biochem. Sci.*, **26**, 438–444.
3. Ishii,Y. and Yanagida,T. (2000) Single molecule detection in life sciences. *Single Mol.*, **1**, 5–16.
4. Ha,T. (2001) Single-molecule fluorescence methods for the study of nucleic acids. *Curr. Opin. Struct. Biol.*, **11**, 287–292.
5. Weiss,S. (2000) Measuring conformational dynamics of biomolecules by single molecule fluorescence spectroscopy. *Nature Struct. Biol.*, **7**, 724–729.
6. Ha,T. (2001) Single-molecule fluorescence resonance energy transfer. *Methods*, **25**, 78–86.
7. Weber,M.A., Stracke,F. and Meixner,A.J. (1999) Dynamics of single molecules observed by confocal imaging and spectroscopy. *Cytometry*, **36**, 217–223.
8. Hansma,H.G., Kim,K.J., Laney,D.E., Garcia,R.A., Argaman,M., Allen,M.J. and Parsons,S.M. (1997) Properties of biomolecules measured from atomic force microscope images: a review. *J. Struct. Biol.*, **119**, 99–108.
9. Hansma,H.G. (2001) Surface biology of DNA by atomic force microscopy. *Annu. Rev. Phys. Chem.*, **52**, 71–92.
10. Engel,A., Lyubchenko,Y. and Müller,D. (1999) Atomic force microscopy: a powerful tool to observe biomolecules at work. *Trends Cell Biol.*, **9**, 77–80.
11. Betzig,E. and Chichester,R.J. (1993) Single molecules observed by near-field scanning optical microscopy. *Science*, **262**, 1422–1425.
12. Meixner,A.J. and Kneppe,H. (1998) Scanning near-field optical microscopy in cell biology and microbiology. *Cell. Mol. Biol.*, **44**, 673–688.
13. Peterman,E.J.G., Brasselet,S. and Moerner,W.E. (1999) The fluorescence dynamics of single molecules of green fluorescent protein. *J. Phys. Chem.*, **103A**, 10553–1056.
14. Brasselet,S., Peterman,E.J.G., Miyawaki,A. and Moerner,W.E. (2000) Single-molecule fluorescence resonant energy transfer in calcium concentration dependent cameleon. *J. Phys. Chem.*, **104B**, 3676–3682.
15. Kubitscheck,U., Kückmann,O., Kues,T. and Peters,R. (2000) Imaging and tracking of single GFP molecules in solution. *Biophys. J.*, **78**, 2170–2179.
16. Moerner,W.E., Peterman,E.J.G., Brasselet,S., Kummer,S. and Dickson,R.M. (1999) Optical methods for exploring dynamics of single copies of green fluorescent protein. *Cytometry*, **36**, 232–238.
17. Sugasawa,K., Ng,J., Masutani,C., van der Spek,P.J., Eker,A.P.M., Hanaoka,F., Bootsma,D. and Hoeijmakers,J.H.J. (1998) Xeroderma pigmentosum group C protein complex is the initiator of global genome nucleotide excision repair. *Mol. Cell*, **2**, 223–232.
18. Houtsmuller,A.B., Rademakers,S., Nigg,A.L., Hoogstraten,D., Hoeijmakers,J.H. and Vermeulen,W. (1999) Action of DNA repair endonuclease ERCC1/XPF in living cells. *Science*, **284**, 958–961.
19. de Laat,W.L., Jaspers,N.G.J. and Hoeijmakers,J.H.J. (1999) Molecular mechanism of nucleotide excision repair. *Genes Dev.*, **13**, 768–785.
20. Araujo,S.J. and Wood,R.D. (1999) Protein complexes in nucleotide excision repair. *Mutat. Res.*, **435**, 23–33.
21. Matsunaga,T., Park,C.H., Bessho,T., Mu,D. and Sancar,A. (1996) Replication protein A confers structure-specific endonuclease activities to the XPF-ERCC1 and XPG subunits of human DNA repair excision nuclease. *J. Biol. Chem.*, **271**, 11047–11050.
22. Hey,T., Lipps,G. and Krauss,G. (2001) Binding of XPA and RPA to damaged DNA investigated by fluorescence anisotropy. *Biochemistry*, **40**, 2901–2910.
23. Buschta-Hedayat,N., Buterin,T., Hess,M.T., Missura,M. and Naegeli,H. (1999) Recognition of nonhybridizing base pairs during nucleotide excision repair of DNA. *Proc. Natl Acad. Sci. USA*, **96**, 6090–6095.
24. Li,L., Peterson,C.A., Lu,X. and Legerski,R.J. (1995) Mutations in XPA that prevent association with ERCC1 are defective in nucleotide excision repair. *Mol. Cell. Biol.*, **15**, 1993–1998.
25. Mu,D., Wakasugi,M., Hsu,D.S. and Sancar,A. (1997) Characterization of reaction intermediates of human excision repair nuclease. *J. Biol. Chem.*, **272**, 28971–28979.
26. Stigger,E., Drissi,R. and Lee,S.-H. (1998) Functional analysis of human replication protein A in nucleotide excision repair. *J. Biol. Chem.*, **273**, 9337–9343.

27. Jones,C.J. and Wood,R.D. (1993) Preferential binding of the xeroderma pigmentosum group A complementing protein to damaged DNA. *Biochemistry*, **32**, 12096–12104.
28. Wang,M., Mahrenholz,A. and Lee,S.-H. (2000) RPA stabilizes the XPA-damaged DNA complex through protein-protein interaction. *Biochemistry*, **39**, 6433–6439.
29. Wakasugi,M. and Sancar,A. (1999) Order of assembly of human DNA repair excision nuclease. *J. Biol. Chem.*, **274**, 18759–18768.
30. Hoeijmakers,J.H.J. (2001) Genome maintenance mechanisms for preventing cancer. *Nature*, **411**, 366–374.
31. Henricksen,L.A., Umbricht,C.B. and Wold,M.S. (1994) Recombinant replication protein A: expression, complex formation and functional characterization. *J. Biol. Chem.*, **269**, 11121–11132.
32. de Laat,W.L., Appeldoorn,E., Sugasawa,K., Weterings,E., Jaspers,N.G. and Hoeijmakers,J.H. (1998) DNA-binding polarity of human replication protein A positions nucleases in nucleotide excision repair. *Genes Dev.*, **12**, 2598–2609.
33. Vermeulen,W., van Vuuren,A.J., Chipoulet,M., Schaeffer,L., Appeldoorn,E., Weeda,G., Jaspers,N.G., Priestley,A., Arlett,C.F., Lehmann,A.R. *et al*. (1994) Three unusual repair deficiencies associated with transcription factor BTF2(TFIIH): evidence for the existence of a transcription syndrome. *Cold Spring Harbor Symp. Quant. Biol.*, **59**, 317–329.
34. Eker,A.P., Vermeulen,W., Miura,N., Tanaka,K., Jaspers,N.G., Hoeijmakers,J.H. and Bootsma,D. (1992) Xeroderma pigmentosum group A correcting protein from calf thymus. *Mutat. Res.* **274**, 211–24.
35. Garcia-Parajo,M.F., Veerman,J.-A., Segers-Nolten,G.M.J., de Grooth,B.G., Greve,J. and van Hulst,N.F. (1999) Visualising individual green fluorescent proteins with a near field optical microscope. *Cytometry*, **36**, 239–246.
36. Garcia-Parajo,M.F., Segers-Nolten,G.M.J., Veerman,J.-A., Greve,J. and van Hulst,N.F. (2000) Real-time light-driven dynamics of the fluorescence emission in single green fluorescent protein molecules. *Proc. Natl Acad. Sci. USA*, **97**, 7237–7242.
37. Dickson,R.M., Cubitt,A.B., Tsien,R.Y. and Moerner,W.E. (1997) On/off blinking and switching behaviour of single molecules of green fluorescent protein. *Nature*, **388**, 355–358.
38. He,Z., Henricksen,L.A., Wold,M.S. and Ingles,C.J. (1995) RPA involvement in the damage-recognition and incision steps of nucleotide excision repair. *Nature*, **374**, 566–569.
39. Patrick,S.M. and Turchi,J.J. (2002) Xeroderma pigmentosum complementation group A protein (XPA) modulates RPA-DNA interactions via enhanced complex stability and inhibition of strand separation activity. *J. Biol. Chem.*, **277**, 16096–16101.
40. Iakoucheva,L.M., Walker,R.K., van Houten,B. and Ackerman,E.J. (2002) Equilibrium and stop-flow kinetic studies of fluorescently labeled DNA substrates with DNA repair proteins XPA and replication protein A. *Biochemistry*, **41**, 131–143.
41. Kim,C., Paulus,B.F. and Wold,M.S. (1994) Interactions of human replication protein A with oligonucleotides. *Biochemistry*, **33**, 14197–14206.
42. Lu,H.P., Iakoucheva,L.M. and Ackerman,E.J. (2001) Single-molecule conformational dynamics of fluctuating noncovalent DNA-protein interactions in DNA damage recognition. *J. Am. Chem. Soc.*, **123**, 9184–9185.